Experimental study of ceramic coatings on lower-density ceramic substrates

C. I. Torres[1,2]*, C. P. Miquelarena[2], G. L. Bianchi[1,3]
[1]Energy and Environmental Innovation Group, Malvinas Institute, Faculty of Engineering,
National University of La Plata, 372 Diagonal 80, La Plata, Argentina
[2]Center for Technology of Mineral Resources and Ceramics, Gonnet, Argentina
[3]National Council for Scientific and Technical Research, Buenos Aires, Argentina

Abstract

Adhesion and homogeneity of the coating-substrate were analyzed on the basis of the establishment of coating mineralogy. Substrate raw materials used were kaolin clay and a calcined alumina 4 μm; a series of higher density ceramic coatings were deposited using calcined aluminas 0.5 μm and 4 μm, silica fume, and talc. The dip coating technique was applied to all substrates and later sintered at 1300 ºC. Shrinkage and density of coatings mixtures and substrate were separately evaluated. X-ray diffraction was utilized to identify the crystalline phases present in the coatings, while optical and electron microscopy were employed for the structural characterization of the coatings. Coatings exhibited lower shrinkage compared to the substrate. Among the specimens that exhibited good adhesion, cracks were observed to extend parallel to the substrate surface. The presence of cristobalite on the coating indicated that the failure mechanism involved buckling. The crack dimension presented on the coating decreased after adding talc to the mixture.
Keywords: Al_2O_3-SiO_2-MgO, dip coating, clay substrate, sintering effort, brittle fracture.

INTRODUCTION

Ceramic coatings have attracted a great deal of interest as they can develop interesting properties, such as high-temperature strength [1-3], improvement of chemical attack [4, 5], and water infiltration resistance [6-8]. There are several studies on the application of a ceramic coating to reinforce mechanical strength [9-11]. Hard ceramic coatings have a wide range of applications, such as turbine blades [12], furnace bricks [5], and pipelines [13]. In addition, functionally gradient materials (FGMs) have been developed to meet the requirement of certain materials for a continuously varying property, such as hardness, dielectric constant, or thermal resistance, from one surface to the other. These FGMs have a compositional gradient, composed of ceramic-ceramic or ceramic-metal from one surface of the material to the other [14]. Ceramic coatings such as alumina are sought after in applications requiring dense, high-quality layers for protection against oxidation and corrosion as well as for thermal barrier coatings [15]. The mechanical properties of ceramics have a strong correlation with the density. By making the density of the coating higher than that of the substrate, the coating is mechanically stronger. In order to enhance the surface properties of the specimen, a dense coating is applied to the substrate, resulting in a material with improved mechanical strength and the ability to meet high strength requirements. Stress during the sintering process occurs as a result of different contraction coefficients for coating and substrate. As a result of stress, brittle fracture cracks appear on the interface due to a difference in the shrinkage level of the two elements of the coated material. The stresses generated depend upon the thickness and the composition of the coating [16].

Ceramic coatings were manufactured using a different mixture of calcined alumina with a particle size of 0.5 μm (calcined alumina 0.5 μm) and calcined alumina with a particle size of 4 μm (calcined alumina 4 μm), silica fume and talc. High reactivity calcined alumina 0.5 μm is used as its sintering temperature is similar to that of the substrate material. This alumina has a micro-sized particle allowing higher densities at lower temperatures [17, 18]. Calcined alumina 4 μm has a particle size approximately 8 times larger than that of calcined alumina 0.5 μm, but calcined alumina 0.5 μm has high sintered density. The goal is to reach a lower density after the sintering process, and using a proper ratio of calcined alumina 0.5 and 4 μm makes the control of the final density easier to compare to the substrate material. Studies have been conducted using different alumina particle sizes to observe the drying shrinkage behavior and the final porosity [19, 20]. These factors influence both the material sintering and the degree of compaction achieved. While alumina is the right main material for the coating, adding silica fume to the coating mixture reduces the stress in the sintered alumina that forms rigid crystalline frameworks [21]. Also, silica fume has high reactivity, being amorphous at first,

---

*camila.torres@ing.unlp.edu.ar
https://orcid.org/0000-0003-1227-9478

and completely crystallizing at high temperatures, allowing better contact between the substrate and the coating [16]. The porosity after the sintering of silica fume is of the order of the nano-scale due to its small size [22].

Previous studies have shown that the similarity of structures and types of intercrystalline bonds between the substrate and coating is crucial for improved adhesion [23]. To enhance adherence, one potential solution is to align the mineralogical composition of both materials via sintering. This can be achieved by utilizing a starting chemistry composition for the coating that closely resembles that of the substrate. In that sense, MgO is presented in most chemistry compositions of clays and it is frequently used in alumina materials to increase its densification [24-27]. One possible way to incorporate MgO is through talc. In order for the specimen to be completed, a series of variations of coating mixtures were deposited on the substrate surface. The chosen process was the dip coating technique, which is easy to handle and shows good reproducibility. The dip coating process implies submerging the substrate into a liquid medium (with the coating material), for a certain amount of time, allowing the deposition of a thin layer of the solid suspension that forms the outer surface by solidification [11, 28]. After drying, the specimen is sintered at sintering temperature. The materials used for the substrate are: 'blend' type kaolin clay and calcined alumina 4 μm. The substrate was made through a molding process into cylinders which allows easier coating techniques. The cylindrical geometry, in its cross-section, generates stress on its surface during sintering that has an angular direction [29]. As can be noted, the coating is tensioned by tensile stresses, generating cracks on its surface.

The objectives of this work were to establish a proper ratio between calcined alumina 0.5 μm and calcined alumina 4 μm, to promote adherence between the substrate and coating by assimilating the starting chemistry composition of both materials, to study different ratios of the coating solid mixtures for the homogeneity improvement of the coated system, and to determine the failure mode after sintering of the specimens coated with different composition of solid mixtures. Chemical compounds were added to the coating solid mixture to match the properties of the substrate material. The density and contraction of the coating solid mixtures and substrate were measured due to the sintering of the specimens. Identification of crystalline phases of the sintered coating mixtures was made by X-ray diffraction. The coated systems' failure as a result of the sintering effort was analyzed by optical microscopy. Coated systems were obtained by dip coating a low-density substrate. The production of high-density surface-sintered coatings produced utilizing low-density ceramic substrates is a promising field of research with potential applications in technology, including serving as ceramic supports for fuel cells and as ceramic catalyst supports.

MATERIALS AND METHODS

Materials: substrate was made from commercial 'blend' kaolin clay (Piedra Grande, Neuquen, Argentina), and calcined alumina 4 μm (A2G, Almatis), using a ratio of 80 wt% of blend clay and 20 wt% of calcined alumina 4 μm for the mixture. The coating material was made of mixtures of calcined alumina 0.5 μm (A16, Almatis), calcined alumina 4 μm, the same used for the substrate, silica fume, and talc. The chemical and mineralogical composition of kaolin clay is presented in Table I. The chemical composition was determined by X-ray fluorescence spectroscopy (XRF), using an energy dispersive spectrometer (EDX-800 HS, Shimadzu) on samples dried at 110 °C. The chemical analysis was performed to determine the average value and standard deviation of the weight percentages of the oxides present in the clay sample. The mineralogical phases were identified by X-ray diffraction (XRD), using a diffractometer (PW3710, Philips) in the range from 5° to 70° with a step of 0.04° and a permanence of 2 s/step. The mineralogical composition was determined by applying the Rietveld method and Fullprof structural refinement program to the XRD pattern. The characteristics of calcined alumina 4 μm A2G powder were as follows: α-alumina, purity 99.1%, and mean particle size 4 μm. The characteristics of calcined alumina 0.5 μm A16 powder were as follows: α-alumina, purity 99.8%, mean particle size 0.5 μm. Table II presents the chemical composition, mean particle size, the specific surface area of silica fume and talc, as well as the mineralogical composition of talc.

Table I - Average values (± standard deviation) of chemical and mineralogical compositions of blend kaolin clay.

Chemical composition (wt%)	
SiO_2	55.0±0.5
Al_2O_3	28.6±0.5
Fe_2O_3	4.1±0.5
MgO	0.7±0.5
K_2O	2.3±0.5
TiO_2	0.8±0.5
CaO	0.2±0.5
LOI	8.1±0.1
Mineralogical composition (wt%)	
Quartz	25
Kaolinite	55
Illite	13
Plagioclase	2
Potassium feldspar	5

Preparation of the substrate: substrate was made by mixing the blend kaolin clay and calcined alumina 4 μm in a wet ball mill for 2 h (using 20 mm diameter balls). After the milling, the mixture was dehumidified in a plaster cast mold until its plasticity allowed the molding of the clay. The cylinder was made by extruding the paste, obtaining a 7 mm diameter and 15 mm high cylindrical substrate. Close attention was drawn to this process so as to keep a smooth surface free of imperfections and thus avoid failure

Table II - Chemical and mineralogical compositions, mean particle size (PS), and specific surface area (SSA) of talc and silica fume.

RM	Chemical composition (wt%)										Mineral. comp. (wt%)			PS (μm)	SSA (m^2/g)
	SiO$_2$	MgO	Al$_2$O$_3$	CaO	Fe$_2$O$_3$	K$_2$O	Na$_2$O	C*	FeO	LOI	Talc	Zeolite	FA		
Talc	52.0	32.5	0.5	0.8	-	-	-	-	0.7	13	93	5	2	14.0	1.0
Silica	96.5[a]	0.5[b]	0.7[b]	0.4[b]	0.3[b]	0.9[b]	0.3[b]	0.8[b]	-	1.5[b]	-	-	-	0.1	40.0

*RM: raw material; *: free C; LOI: loss on ignition; FA: ferro-actinolite; [a]: minimum; [b]: maximum.*

initiation. Before the coating deposition, each piece was calcined at 600 °C to remove interstitial water and organics that would otherwise pass through the coating, producing their cracking.

Preparation of the suspensions: different types of suspensions were prepared by slowly adding the solids mixture into distilled water (pH 9) until the concentration reached 50 wt%; the process was made under ultrasound and magnetic agitation. As a dispersant of calcined alumina 0.5 μm A16, Dolapix 64 was used at 0.5% weight by weight of calcined alumina 0.5 μm [30]. The 50 wt% concentration allowed a homogeneous deposition on the surface of the substrate without macro detachment observed and was established by experimental observation.

Composition of the suspensions: nine types of suspension for the coating were made using different mixtures of solids with different ratios, 50 wt% was set for each one. The suspension composition of the coatings was selected and the percentages studied were adjusted by experimental observation. The first three suspension mixtures were made of different alumina ratios of calcined alumina 0.5 μm/4 μm (called AAi, i=1,2,3). The ratios used for this study were: 95 wt% calcined alumina 0.5 μm and 5 wt% calcined alumina 4 μm, AA1; 85 wt% calcined alumina 0.5 μm and 15 wt% calcined alumina 4 μm, AA2; and 70 wt% calcined alumina 0.5 μm and 30 wt% calcined alumina 4 μm, AA3. After observing the coating behavior of these three first coatings mixtures, a proper ratio was determined. The reason why the coating made with AA1 had the best performance among these three solids mixtures is discussed in the results section of this work. Three new mixtures were made, all using the base ratio AA1 (called A) and adding different proportions of silica fume (called S). These three new composition mixtures were called ASi, i=1,2,3. The values of the percentages of AA1 and S used are reported in Table III. Finally, a percentage of AA1 was replaced by talc (called T), obtaining another three composition mixtures, called ASTi, i=1,2,3. The incorporation was made by taking a 10 wt% of AA1 to the solid mixture ASi and it was replaced by talc. The values of the percentages of AA1, S, and T used are reported in Table III.

Coating deposition: once the different suspensions were made, and the substrate was calcined, one cylindrical substrate was immersed for 10 s once in the designated suspension. 10 s and one cycle were effective to provide a homogeneous and uniform deposit of the suspension on the substrate surface. Each submerged specimen was dried on

Table III - Compositions (wt%) of the solid mixtures of the dip-coating suspensions with AA1 (95/5 calcined alumina 0.5 μm/4 μm), S (silica fume), and T (talc).

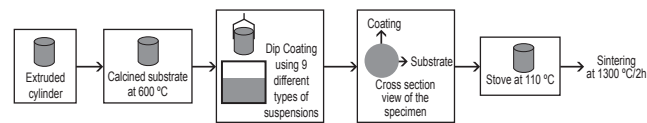| Sample	AA1	S	T
AS1	97	3	-
AS2	95	5	-
AS3	90	10	-
AST1	87	3	10
AST2	85	5	10
AST3	80	10	10

Figure 1: Process of application of the coating on the substrate surface.

a stove at 110 °C for 30 min. Fig. 1 shows the coating application process.

Sintering conditions: the sintering of the specimens was carried out in an electric furnace (MHI) at 1300 °C in an air atmosphere, with a ramp of 5 °C /min and a dwell of 2 h. Afterward, cooling was carried out until room temperature.

Characterization of the substrate and the coating solid mixtures: the identification of the phases of the sintered samples AS and AST was carried out using the same method as described for the mineralogical composition of the kaolin clay. A dilatometric test was performed on the substrate and on the coating material separately, for the compositions ASi and ASTi, i=1,2,3. For the substrate dilatometric test, a piece of uncoated base material was rectified. The AS and AST coating samples were prepared from the remaining suspension of the dip-coating process, which was poured into a plaster cast and left to dry, obtaining a cylindrical geometry that was then rectified. A dilatometer (TMA 8311, Rigaku) was used, using a ramp of 10 °C/min up to 1300 °C and a 1 h dwell. The final temperature in the dilatometric test was the same as the sintering temperature of the specimens. Substrate and coating densities were measured separately; the coating sample preparation was similar to that described in the dilatometric test. The Archimedes method in kerosene

and water was used for green (non-sintered) and sintered, respectively, for both substrate and coating [23]. The density of each composition sample was measured on five occasions, resulting in five individual measurements. Each sample was prepared and tested five times, and the density was measured in each instance. The average and standard deviation were subsequently calculated from the collected data. These average density measurements allowed for the evaluation of the density behavior of the coated material through a series of calculations based on the density (ϱ) results. The densification percentage was calculated by:

$$Densification = \left(\frac{\rho_{s,c}}{\rho_{s,c}} - 1\right).100 \qquad (A)$$

where $\varrho_{g,c}$ and $\varrho_{s,c}$ are, respectively, the green and sintered densities of the coating. The change in chemical composition can produce a density change with respect to an alumina coating. The percentage density decrease was calculated by:

$$Densification\ decrease = \left(1 - \frac{\rho_{s,c}}{\rho_{s,A16}}\right).100 \qquad (B)$$

where $\varrho_{s,A16}$ is the density of the sintered alumina 0.5 μm (3.22 g/cm^3) as reference. The difference in density that existed between the coating and the substrate for each chemical composition was determined. The density difference percentage was calculated by:

$$Densification\ difference = \left(\frac{\rho_{s,c}}{\rho_{s,s}} - 1\right).100 \qquad (C)$$

where $\varrho_{s,s}$ is the average density of the sintered substrate as reference.

Preparation of the specimens for analysis and coating characterization: the specimens in vertical position were embedded in resin, then ground and polished with SiC abrasive paper up to 1000 mesh. The polished cross-section morphologies of the coating-substrate system were characterized by scanning electron microscopy (SEM, JCM 6000, Jeol) and optical microscopy (BX60, Olympus). Crack

width and coating thickness were measured using the SEM scale bar; five measurements of each magnitude were taken and then the average was calculated.

RESULTS AND DISCUSSION

The chemical composition of the substrate (Table I) was used as the base for selecting the material coating, to make compatible the chemical composition of both materials. Al_2O_3 was the main material of the coating as it shows higher density than that of SiO_2. Then, SiO_2 was chosen as a coating material because it is the main chemical compound of the substrate. At this point, the chemical compounds left to choose from were MgO and TiO_2, since both are used to reduce the sintering temperature of Al_2O_3. In addition, they promote the crystallization of magnesium aluminate spinel and mullite [25]. The other chemical compounds present in the substrate composition were not taken into account due to their negative effect on the coating sintered properties [31]. In this study, MgO was incorporated through talc due to its wide availability. The results obtained for the different percentages of the selected chemical compounds and the behavior of the coated system are detailed below.

XRD of AS and AST samples: in Fig. 2a XRD patterns of AS1 (97/3 A/S), AS2 (95/5 A/S), and AS3 (90/10 A/S) sintered samples are shown. It was observed that alumina (Al_2O_3), in the form of corundum, and cristobalite were the only phases. The peak of cristobalite (SiO_2) increased in the following order: AS1, AS2, and AS3. This resulted directly from the increase in the percentage of S (silica fume) in the solid mixture. In Fig. 2b XRD patterns of AST1 (87/3/10 A/S/T), AST2 (85/5/10 A/S/T) and AST3 (80/10/10 A/S/T) sintered samples are shown. The peak of cristobalite was no longer significant because silica and alumina began to react with talc aggregate. The phases observed were: alumina, in the form of corundum, cristobalite, sapphirine, mullite, and cordierite. AST2 had the highest intensity peaks for sapphirine ($7MgO.9Al_2O_3.3SiO_2$). AST3 had the highest peaks of mullite ($3Al_2O_3.2SiO_2$) and cordierite ($2MgO.2Al_2O_3.5SiO_2$). XRD patterns of AST samples
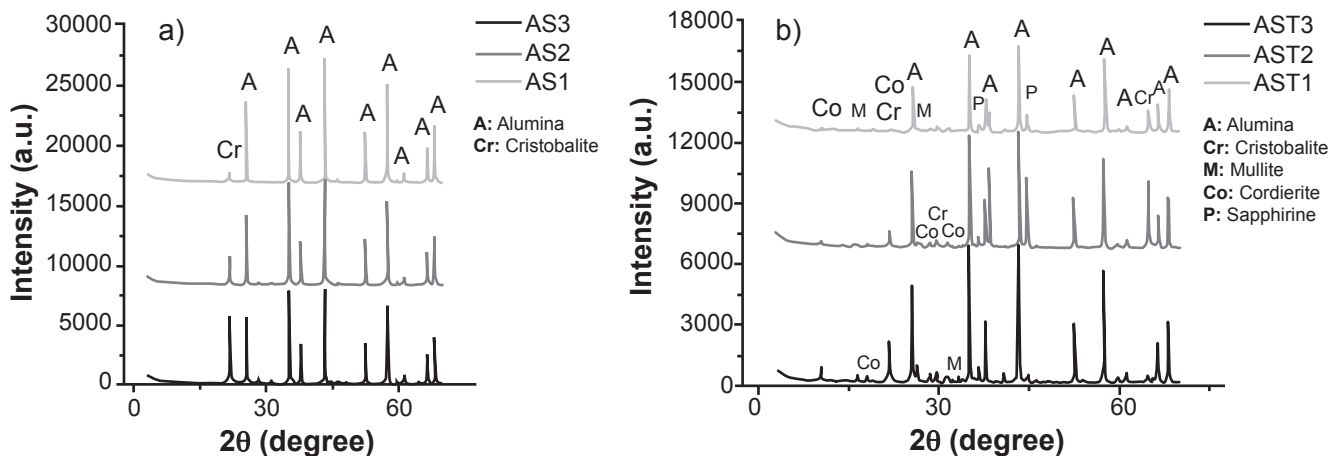

Figure 2: XRD patterns of the samples sintered at 1300 °C/2 h: a) AS; and b) AST

showed no band located between 20-30° 2θ, assigned to the non-crystalline silicate phase, which would be produced by the melting of SiO_2 [32], being this one of the chemical compounds added to the coating solid mixture. The vitreous phase would be generated by two main factors: either the sintering temperature is in the melting point of SiO_2 or the presence of chemical compounds that reduces the temperature of melting. In this study, the temperature did not reach the melting point of SiO_2, but chemical compounds were added to the solid mixture. FeO, Fe_2O_3, and CaO were incorporated because of the addition of talc and silica fume. Similarly, the incorporation of K_2O and Na_2O was a result of the addition of silica fume. These oxides significantly reduce the melting temperature of SiO_2 [33]. However, the four oxides were found at a low percentage, less than 0.7 wt% in the solid mixture. This low concentration was insufficient to produce a vitreous phase, which is undesirable as it reduces the mechanical strength of the coating material [31].

Dilatometric test of AS, AST, and substrate samples: the results of dilatometry of ASi, i=1,2,3, and the base material are shown in Fig. 3a. It was observed that at the end of the test, the contraction, in absolute value, decreased with the increase in S percentage, being 2.20%, 1.40% and 1.20% for AS1, AS2, and AS3 ratios, respectively. This was due to the increased reactivity of alumina compared to the silica fume. Also, in Fig. 3a it can be observed that at the end of the test, the contraction for the substrate was 7% in absolute value. The results of dilatometry of ASTi, i=1,2,3, and the base material are shown in Fig. 3b. It was observed that at the end of the test the contraction, in absolute value, increased with the increase in S percentage, being 1.80%, 2.60% and 3.00% for AST1, AST2, and AST3 ratios, respectively; this was due to the increase in reactivity between alumina and silica fume in presence of talc. The dilatometry of the substrate showed a slight expansion from room temperature up to the temperature range of 600-650 °C. The curve then flattened up until 900 °C, where contraction occurred slowly between 950-1050 °C. The dilatometry curves of the AS and

AST samples flattened up until 1100 °C, then contraction occurred slowly between 1150-1200 °C.

Density measurements of AA, AS, AST, and substrate samples: Table IV shows the average sintered densities along with their deviations, which were calculated based on five measurements taken for each composition sample, and the percentage of densification, calculated with Eq. A, the density decrease, calculated with Eq. B, and the density difference, calculated with Eq. C, for AA, AS, and AST samples. For the relation AA1, 95/5 (calcined alumina 0.5 μm/4 μm), AA2, 85/15, and AA3, 70/30, it was observed that density and densification decreased in the following order: AA1, AA2, and AA3. It was observed that density and densification decreased as the percentage of calcined alumina 4 μm increased in the solid mixtures. For AA1 the density decrease was 0.6%, and the density difference was approximately 25%. For the relation ASi, i=1,2,3, it was observed that average density and densification decreased as the percentage of S increased in the solid mixtures. This resulted directly from the lower density of the silica compared to that of alumina. It is to be noticed that adding 3 wt% of S in the case of AS1, decreased the density by 9% approximately and reached a density difference of 14.90%. This was due to the low particle size and high specific surface area of S, which were 0.1 μm and 40 m^2/g, respectively (Table II). For the relation ASTi, i=1,2,3, average density values decreased as the percentage of S increased in the solid mixtures. The densification of the AST samples increased as the percentage of S increased. The density decrease for AST2 was 10.50% and the density difference was 12.90%. The other results are shown in Table IV and were not significant for this work.

Characterization of the substrate-coatings: there are four types of failure that may occur in coated systems: delamination of the interface, cracking of the coating, substrate cracking, and buckling [34]. In this work, the specimens presented a mix mode fracture and the main characteristics observed in the coated systems are discussed below. Optical microscopic observations were made for the coated systems, using the
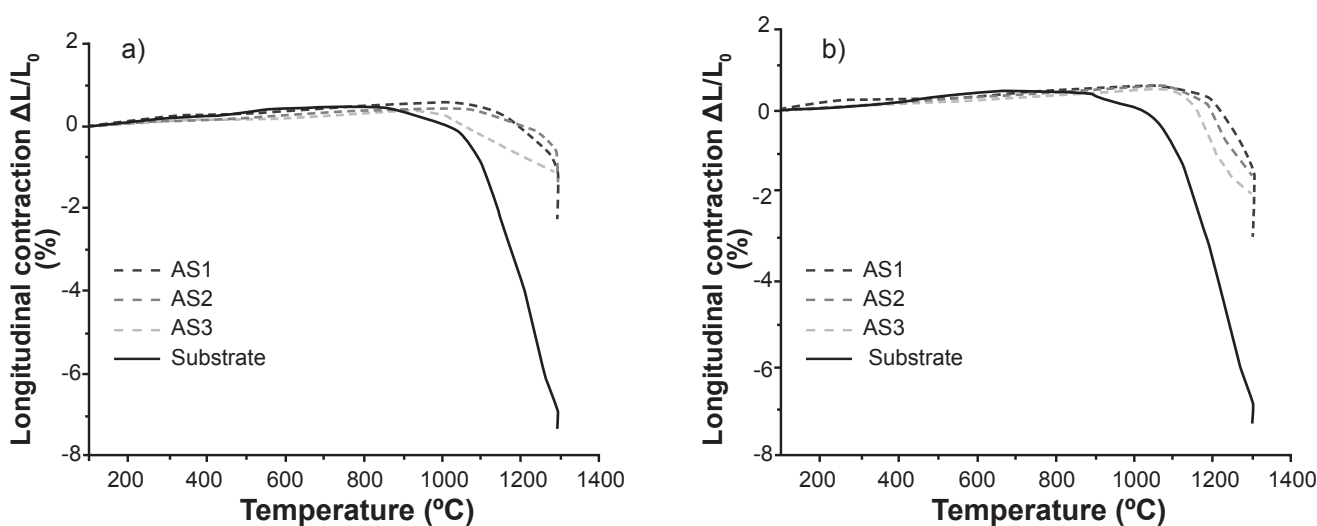

Figure 3: Dilatometric curves of: a) AS samples and substrate; and b) AST samples and substrate.

Table IV - Average density (± standard deviation), densification, density decrease, and density difference for the AA, AS, and AST samples.

Sample*	Sintered density (g/cm³)	Densification (%)	Density decrease (%)	Density difference (%)
AA1	3.21±0.05	28.20	0.60	25.50
AA2	3.17±0.04	23.00	1.50	24.00
AA3	2.98±0.04	15.40	7.50	16.50
AS1	2.93±0.02	15.35	9.00	14.90
AS2	2.69±0.09	12.50	16.50	5.50
AS3	2.68±0.01	12.30	16.70	5.10
AST1	2.95±0.07	16.90	8.40	15.60
AST2	2.88±0.05	18.75	10.50	12.90
AST3	2.80±0.03	18.90	13.00	9.80

*: AA_i=alumina 0.5 µm/4 µm, AS_i=A/S, AST_i=A/S/T.

solid mixtures AA, AS, and AST. Fig. 4 compares the optical images for the coated material with the AA mixtures. It can be observed for the coated samples with AA1 (Fig 4a), AA2 (Fig. 4b), and AA3 (Fig. 4c), that delamination and cracking increased as the percentage of calcined alumina 4 µm increased. The aim of this study was to achieve a coupled layer. Given that with the ratio of alumina AA1 (95/5 calcined alumina 0.5 µm/4 µm) a coating that matched the stated objective was obtained, it was decided that this ratio would be appropriate. For the coated samples with the AS mixtures, it was observed that as the percentage of S increased, delamination increased. The specimen coated with AS1, 97/3 A/S ratio, presented the coating coupled to the substrate. For the specimens coated with AS2 and AS3, 95/5 and 90/10 A/S ratios, respectively, delamination of the coating was observed. Initial analysis suggested that the characteristics of the failure mode of the coated systems using the solid mixtures AS involved buckling of the coating and delamination of the interface. For the coated samples with the AST mixtures, the specimens coated with AST1 and AST3, 87/3/10 and 80/10/10 A/S/T ratios, respectively, presented delamination of the interface, and coupling was not displayed. The specimen coated with AST2, 85/5/10 A/S/T ratio, presented the coating coupled to the substrate. It was registered in the specimens coated with AS and AST solid mixtures substrate cracking. The appearance of

substrate cracks since the chemistry of the coating solid mix changed, with respect to an alumina coating, is explained later in this work. Cross-sectional microscopy observations of the coated samples with the best performance were AS1, for AS solids mixtures, and AST2, for AST solids mixtures. Delamination and cracking were evaluated to determine the best performance of the coated systems, comparing AS and AST samples separately. It was noted that the density difference between substrate and coating values obtained for AS1 and AST2 samples was around 14% (Table IV). If the density of the substrate either increased or decreased, this value would allow control in the difference density, which might be needed for system effective performance.

Analysis by SEM images: Fig. 5 shows SEM images of the specimens coated with AA1, AS1, and AST2. In all the images an area of higher porosity in the substrate and another area of lower porosity in the coating were registered. Fig. 5a shows the specimen coated with AA1. It should be noticed that this coating may not present characteristics of adhesion failure, but experimental observations proved otherwise. The coated samples with the AA mixtures presented severe detachments and areas of uncoated material were exposed. Fig. 5a shows an area with coating, and that the substrate and the coating are coupled. The average coating thickness was 55 µm and the average crack width was 100 µm, the presence of crack was only on the coating. The cohesive
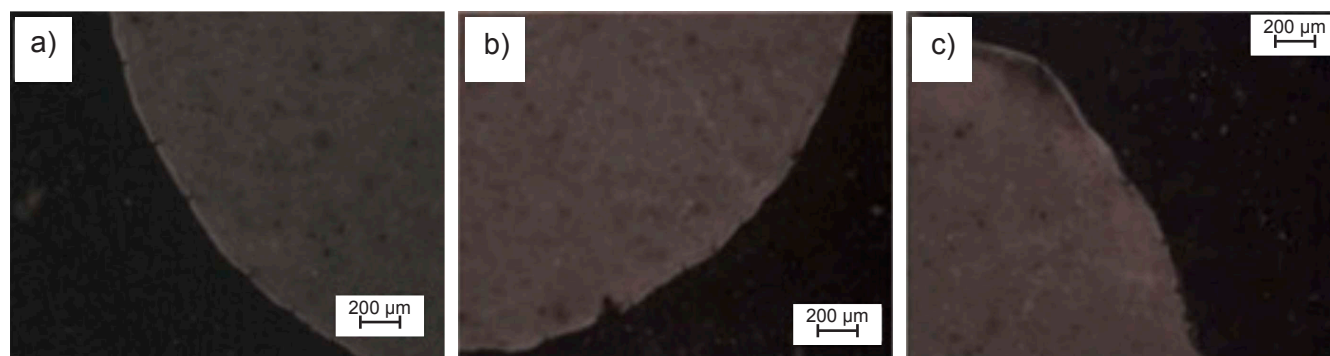

Figure 4: Optical microscope images of specimens coated with: a) AA1 solid mixture, 95/5 (calcined alumina 0.5 µm/4 µm); b) AA2 solid mixture, 85/15; and c) AA3 solid mixture, 70/30.
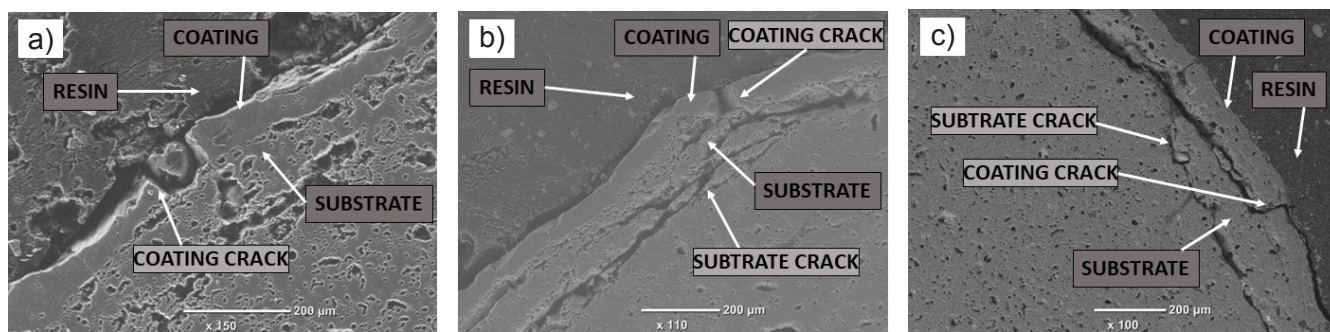
Figure 5: SEM images of specimens coated with: a) AA1 solid mixture; b) AS1 solid mixture; and c) AST2 solid mixture.

failure was spotted only in the coating; this might indicate that the binding energy between the particles was less than the adhesion force with the substrate [1]. In this case, being the substrate was more brittle than the coating, cohesive forces in the substrate were less than in the coating. The crack appeared only in the coating; this gave a good hint of low adhesion. Fig. 5b shows the specimen coated with AS1, with an average coating thickness of 60 μm and average crack width of 50 μm. There is a defect zone in the substrate, caused by cracking of the coating. The cracks, starting at the site of the crack located in the coating and extending to the substrate, propagated parallel to the substrate surface. The approximate lamination depth was 200 μm. To explain the formation of these cracks in the substrate, it is known that the efforts during sintering depend on the coating thickness and its composition [16]. The purpose of this study was to modify the composition but not the thickness of the coating. This implied that the analysis of the substrate cracking was based on the change in the coating composition. Coating breakage is mainly due to tensile stress during sintering. Tensile stresses are perpendicular to compression stresses, and the latter is generated by the different shrinkage of the materials, both coating, and substrate [11]. The chemical composition of an alumina-silica coating caused the behavior to change with regard to an alumina coating, and generated an interface of the coated material; the growth of the crack that originated in the coating by the tensile stress and that extended to the substrate. This substrate failure was triggered by the adhesion between the substrate and the coating, and because the substrate was more brittle than the coating.

Fig. 5c shows the specimen coated with AST2, with an average coating thickness of 75 μm and average crack width of 15 μm, this was about one-third of the value when the AS1 mixture was used. There was a defect zone in the substrate, caused by the cracking of the coating, as a result of the tensile stress generated during the sintering. The observation of cracks originating in the coating and extending to the substrate indicated adhesion at the interface. It can be noted that cracks propagated in a laminar form parallel to the substrate surface and the lamination depth was approximately 200 μm, the same as in the AS1 case. There was a possible explanation that the material coated with the solid mixture AST2 presented a lower crack width than the

coated with mixture AS1. The cristobalite phase has a large volume change (2.8%) from β to α inversion at 220 °C [35]. After exposure to elevated temperature, stress is subjected to compressive stress during cooling, and this results in cracks through the coating layer that leads to spallation [11]. Large stress arises because of compressive stress related to the volume change of cristobalite and is strongly controlled by the initial particle size of silica fume, which was 0.1 μm (Table II), and also by the volume fraction of the volume change phase [36]. During the deposition of the coating by the dip coating technique, the small particle size of the silica fume allowed its distribution between interstitial spaces of calcined alumina 0.5 and 4 μm particles. This resulted in, at the approximate temperature of 220 °C after heat treatment, the volume change of cristobalite on the coating that occurred in an elevated superficial area between alumina grains. The coating made with the solid mixture AS1 presented delamination of the layer. Compressive stress related to the phase transformation of cristobalite can generate the coating layer with circular separation at the interface observed in Fig. 5b. The addition of talc to the coating solid mixture drastically reduced the cristobalite phase on the coating and therefore its crack width.

CONCLUSIONS

The proper ratio of 95 wt% calcined alumina 0.5 μm and 5 wt% calcined alumina 4 μm was determined from the different alumina ratios of these calcined aluminas since the resulting coating had good deposition and lower delamination. No fractures were observed in the substrate. For the different solids mixtures of 95/5 calcined alumina 0.5 μm/4 μm and silica fume, it was observed buckling of the coating and delamination of the interface. This mode of failure relies on the existence of compressive stress within the coating. The coating manufactured with 97 wt% of 95/5 calcined alumina 0.5 μm/4 μm and 3 wt% silica fume had the lowest delamination and its average coating crack width was 50 μm. The adhesion between the substrate and coating was proved by the emergence of a crack, which originated in the coating and extended to the substrate, with a lamination depth of approximately 200 μm. For the different solids mixtures of 95/5 calcined alumina 0.5 μm/4 μm, silica fume, and talc, the coating manufactured with 85 wt% of 95/5

calcined alumina 0.5 μm/4 μm, 5 wt% silica fume and 10 wt% talc (85/5/10 A/S/T ratio) had the lowest delamination. The average coating crack width was 15 μm, improving the homogeneity of the coating compared to the previous case by reducing the crack width. Substrate cracking was observed with a lamination depth of approximately 200 μm. The adhesion of the coated system was maintained. The reduction of the coating crack width, with respect to the previous case, was explained by the drastic decrease in the amount of cristobalite. For the solids mixture 85/5/10 A/S/T ratio, the density decrease was approximately 10% and the contraction was -2.20%. Also, it had the highest XRD peaks of intensity for sapphirine. The density difference value was around 14% for solids mixtures: 97 wt% of 95/5 calcined alumina 0.5 μm/4 μm and 3 wt% silica fume, and 85 wt% of 95/5 calcined alumina 0.5 μm/4 μm, 5 wt% silica fume, and 10 wt% talc. The application of a dense ceramic coating on a ceramic substrate was studied, with the goal of aligning the mineralogical composition of both materials through sintering. However, it was found that full homogeneity of the coating was not attained as a result of dissimilar shrinkage between the coating and substrate. To mitigate this issue, further research into the use of a multilayer coating may provide a viable solution to prevent coating cracks.

REFERENCES

[1] E. Cadavid, F. Vargas-Galvis, M.E. Lopez-Gomez, C. Mesa, F.A. Vargas, G. Latorre, G. Peña, Dyna **85** (2018) 338.
[2] R.D. Kapustin, L.B. Pervukhin, V.S. Vladimirov, S.E. Moizis, Glass Phys. Chem. **34** (2008) 480.
[3] V.T. Mazur, D.C. Chagas, M.M. Mazur, S.A. Pianaro, G. de Vasconcelos, Cerâmica **67**, 383 (2021) 365.
[4] F. Vargas, E. Restrepo, J.E. Rodríguez, F. Vargas, L. Arbeláez, P. Caballero, J. Arias, E. López, G. Latorre, G. Duarte, Ceram. Int. **44** (2018) 3556.
[5] S.A. Zaidan, H.Y. Abed, Eng. Technol. J. **35** (2017) 999.
[6] E.S. Abdrakhimova, V.Z. Abdrakhimov, Inorg. Mater. Appl. Res. **9** (2018) 588.
[7] W. Duan, D. Jia, D. Cai, B. Niu, Z. Yang, Y. Zhou, J. Eur. Ceram. Soc. **41** (2021) 2162.
[8] Y. Sun, D. Cai, Z. Yang, J. Eur. Ceram. Soc. **38** (2018) 4749.
[9] J.M. Martínez, C. Volzone, L.B. Garrido, Appl. Clay. Sci. **149** (2017) 20.
[10] W. Zhang, Q. Ma, K. Zeng, K. Zeng, S. Liang W. Mao, J. Adv. Ceram. **8** (2019) 218.
[11] H. Moon, F.F. Lange, J. Am. Ceram. Soc. **93** (2010) 1264.
[12] T.S. Hille, T.J. Nijdam, A.S.J. Suiker, S. Turteltaub, W. Sloof, Acta Mater. **57** (2009) 2624.
[13] M.A. Zavareh, A.A.D. Mohammed Sarhan, R. Karimzadeh, R. Singh, Ceram. Int. **44** (2018) 5967.
[14] M. Sasaki, T. Hiari, J. Ceram. Soc. Japan **99** (1991) 1002.
[15] D.A. Barrow, T.E. Petroff, M. Sayer, Surf. Coat. Technol. **76** (1995) 113.
[16] M. Touzin, F. Béclin, J. Eur. Ceram. Soc. **31** (2011) 1661.
[17] E. Levänen, T. Mäntylä, J. Eur. Ceram. Soc. **22** (2002) 613.
[18] G.Y. Onoda, L.L. Hench (Eds.), "Ceramic processing before firing", John Wiley Sons (1978).
[19] G. Tari, J.M.F. Ferreira, A.T. Fonseca, Ceram. Int. **25** (1999) 577.
[20] J. Liu, W. Huo, X. Zhang, B. Ren, Y. Li, J. Yang, J. Adv. Ceram. **7** (2018) 89.
[21] M. Bartsch, B. Saruhan, M. Schmücker, H. Schneider, J. Am. Ceram. Soc. **82** (2004) 1388.
[22] J. Liao, P. Gao, L. Xu, J. Feng, J. Adv. Ceram. **7** (2018) 307.
[23] A. Mocciaro, M.B. Lombardi, A.N. Scian, Bol. Soc. Esp. Ceram. V. **56** (2017) 243.
[24] K. Maca, V. Pouchly, K. Bodišová, D. Galusek, J. Eur. Ceram. Soc. **34** (2014) 4363.
[25] H. Yu, Z. Xu, Z. Wei, Y. Chen, J. Li, L. Luo, J. Appl. Ceram. Technol. **15** (2017) 633.
[26] W. Jo, D. Kim, N. Hwang, J. Am. Ceram. Soc. **89** (2006) 2369.
[27] T.T. Parlak, A.S. Demirkiran, J. Adv. Ceram. **7** (2018) 370.
[28] L.E. Scriven, Mat. Res. Soc. Symp. Proc. **121** (1988) 717.
[29] W.D. Kingery, J. Am. Ceram. Soc. **38** (1955) 3.
[30] A. Tsetsekou, C. Agrafiotis, A. Milias, J. Eur. Ceram. Soc. **21** (2001) 363.
[31] M. Sardy, A. Arib, K. El Abbassi, R. Moussa, M. Gomina, New J. Glass Ceram. **2** (2012) 121.
[32] A.K. Chakraborty, *Phase transformation of kaolinite clay*, Springer, India (2014).
[33] C. Zanelli, M. Raimondo, G. Guarini, M. Dondi, J. Non-Cryst. Solids **357** (2011) 3251.
[34] M.D. Thouless, J. Vac. Sci. Technol. **9** (1991) 2510.
[35] A. Aras, Appl. Clay. Sci. **178** (2019) 105126.
[36] L. Luo, X Shan, Y. Guo, C. Zhao, X. Wang, X. Zhao, F, Guo, P. Xiao, J. Am. Ceram. Soc. **101** (2017) 2084.